

Electronic Supporting Information

Toward Heat-tolerant Potassium Batteries based on Pyrolyzed Selenium

Disulfide/ Polyacrylonitrile Positive Electrode and Gel Polymer Electrolyte

Yu Liu,^a Dezhi Yang,^a Weigang Wang,^a Kai Hu,^a Qinghong Huang,^a Yi Zhang,^a Yingchun Miao,^c Lijun Fu*^a, Meng Wu*^b and Yuping Wu*^a

^a State Key Laboratory of Materials-Oriented Chemical Engineering, Institute of Advanced Materials (IAM) and College of Energy Science and Engineering, Nanjing Tech University, Nanjing 211800, China.

^b Fujian Provincial Key Laboratory of Semiconductors and Applications, Collaborative Innovation Center for Optoelectronic Semiconductors and Efficient Devices, Department of Physics, Xiamen University, Xiamen 361005, China.

^c Advanced Analysis and Testing Center, Nanjing Forestry University, Nanjing 210037, China.

*Corresponding Author: l.fu@njtech.edu.cn; lijunfufu@sina.com (L. Fu); meng.wu@xmu.edu.cn (M. Wu); wuyp@njtech.edu.cn (Y. Wu)

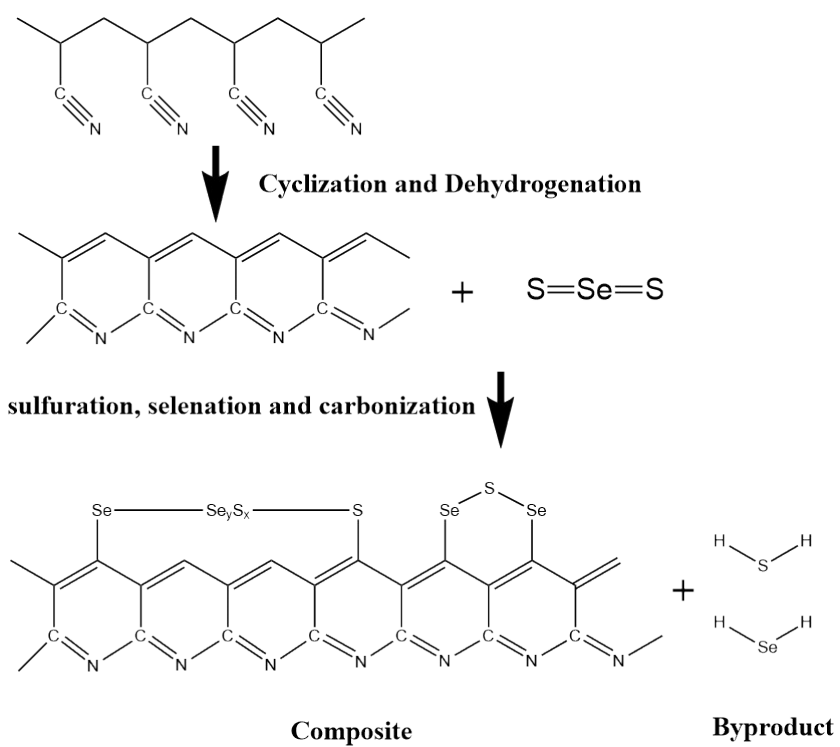


Figure S1. Schematic illustrations of the proposed chemical structure of $\text{SeS}_2\text{-CPAN}$.

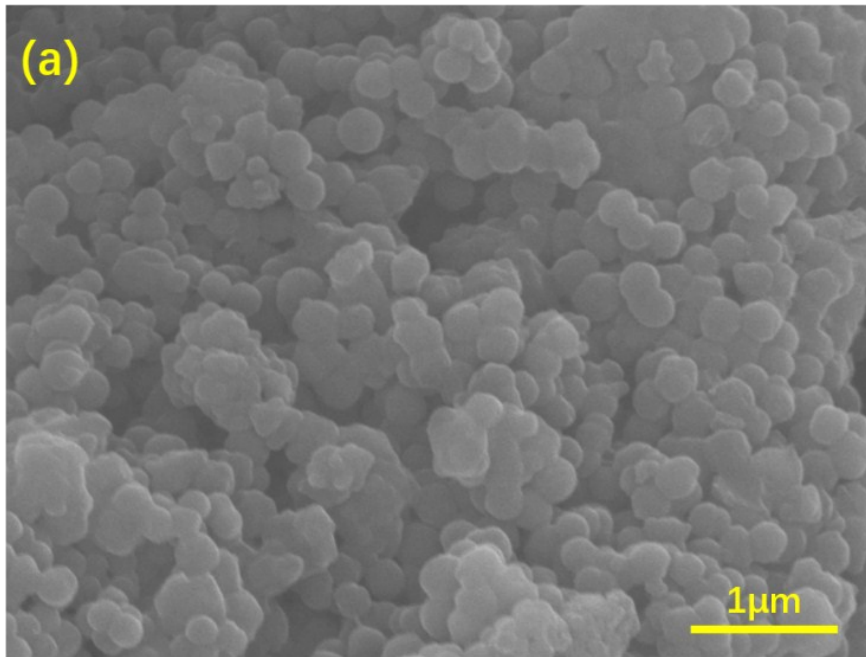


Figure S2. SEM image of SeS₂-CPAN.

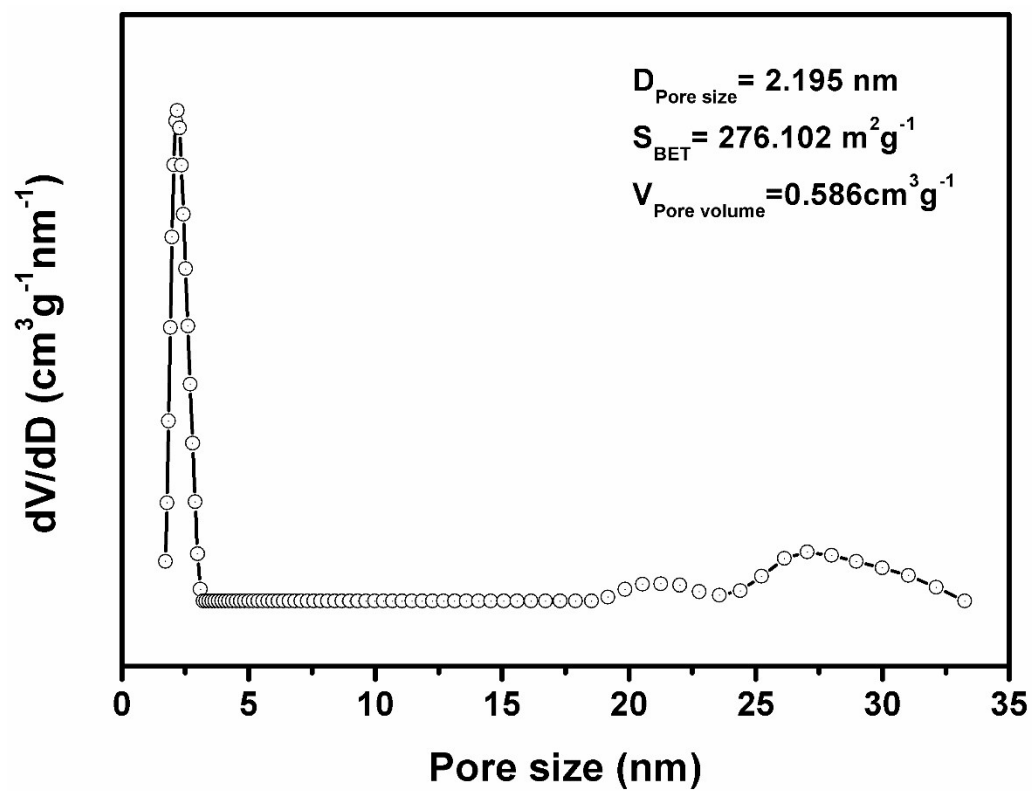


Figure S3. Pore size distribution of SeS₂-CPAN.

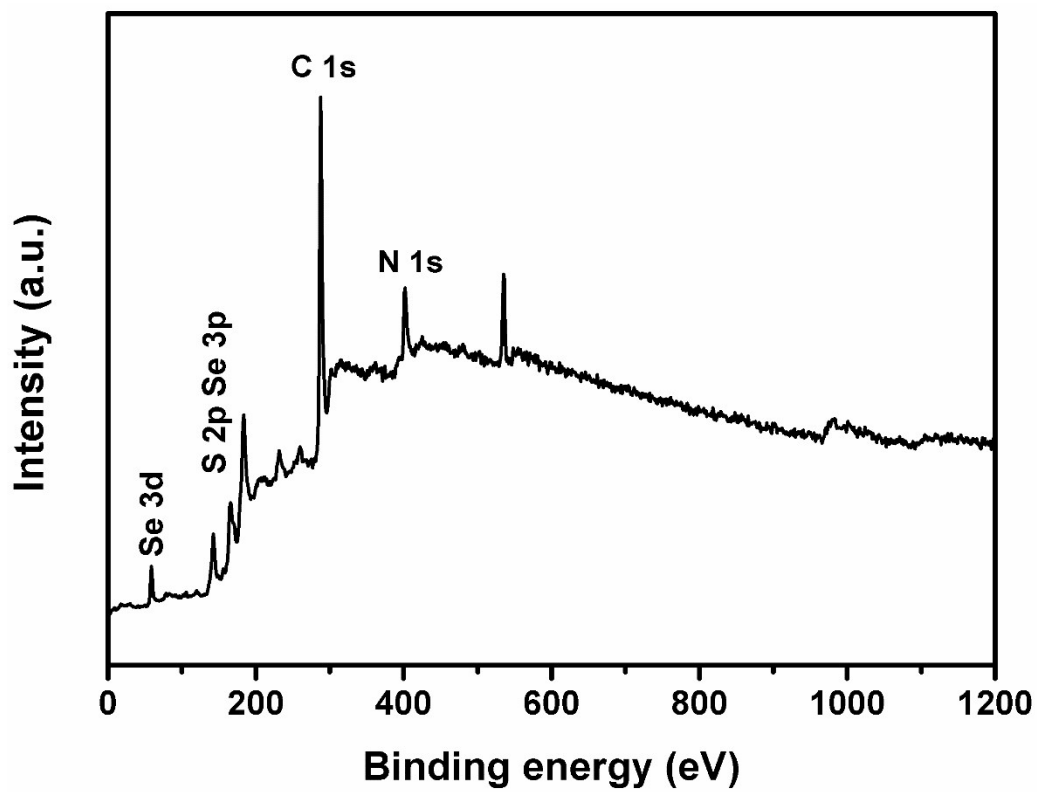


Figure S4. XPS spectrum of SeS₂-CPAN.

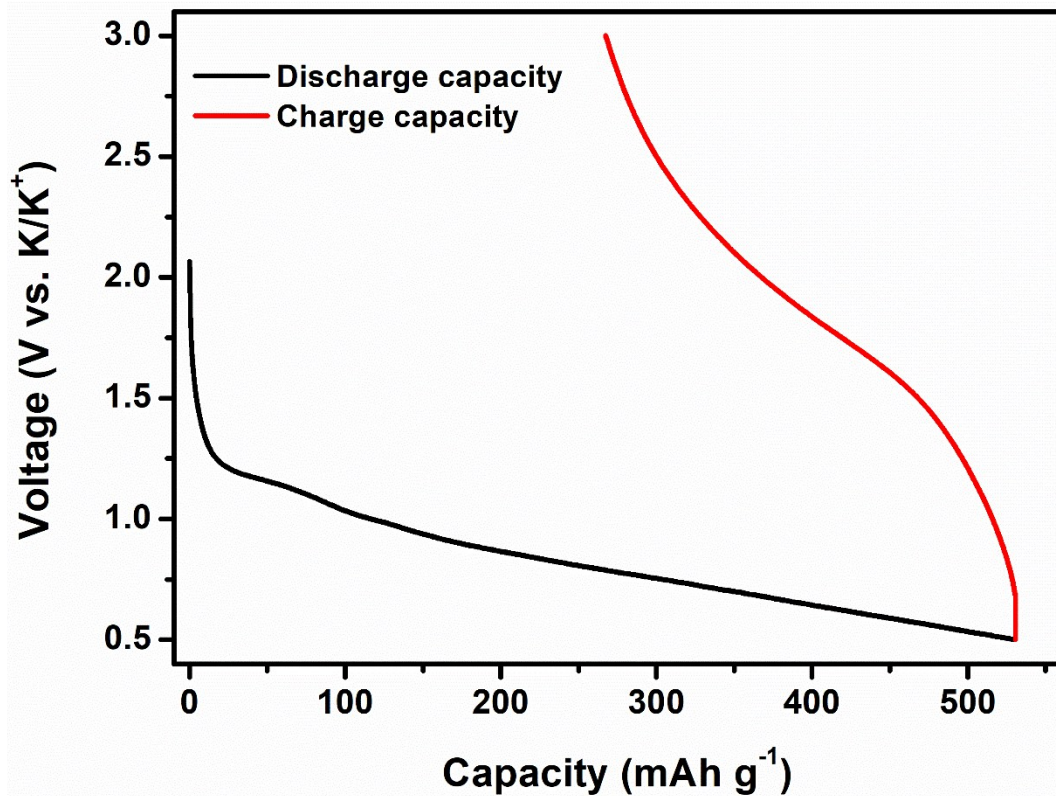


Figure S5. Initial charge and discharge profiles of SeS₂-CPAN for the initial cycles between 0.5 and 3.0 V at 100 mA g⁻¹.

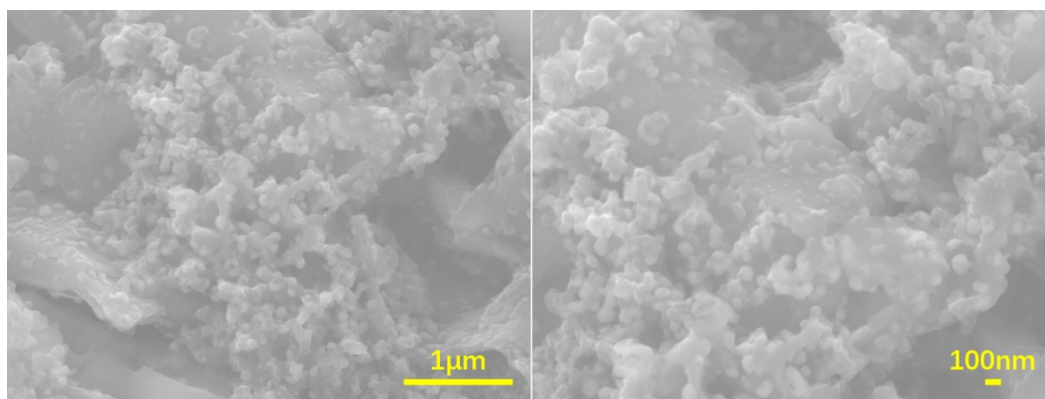


Figure S6. SEM image of the SeS₂-CPAN electrode after 300 cycles.

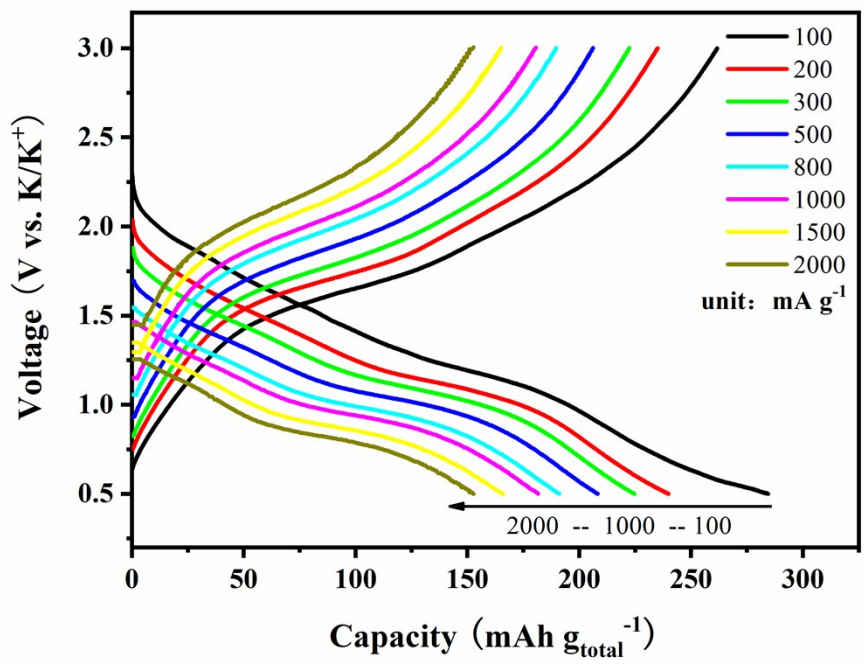


Figure S7. Charge-discharge curves at various current densities.

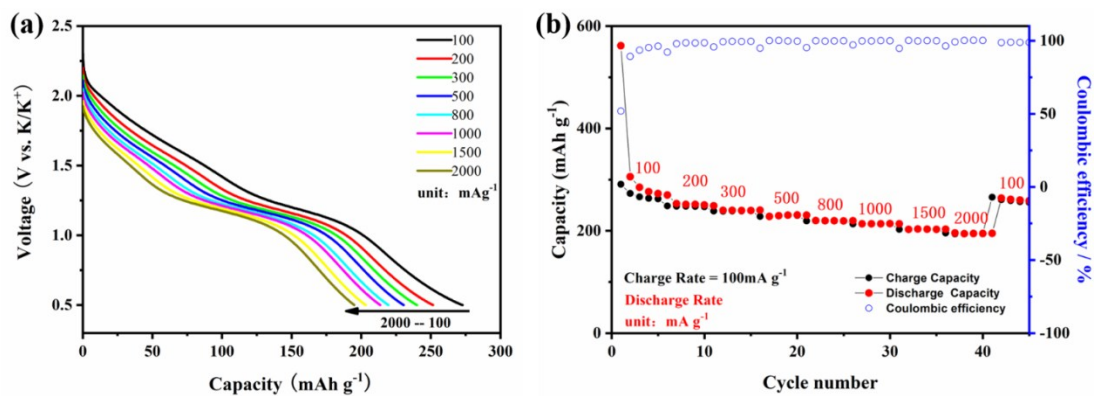


Figure S8. Discharge voltage profiles (a) and cycling performance (b) of SeS₂-CPAN under a constant charge current rate (100 mA g⁻¹) with different discharge current rate from 100 to 2000 mA g⁻¹.

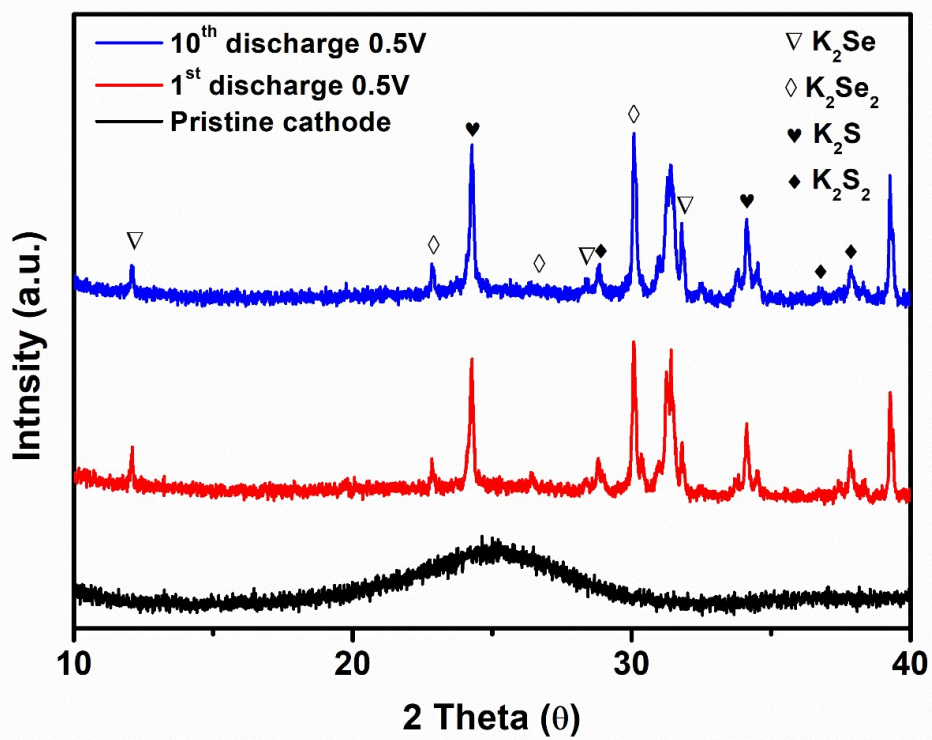


Fig S9. XRD patterns of SeS_2 -CPAN electrode in K-sulfur batteries after the first discharge and the tenth discharge.

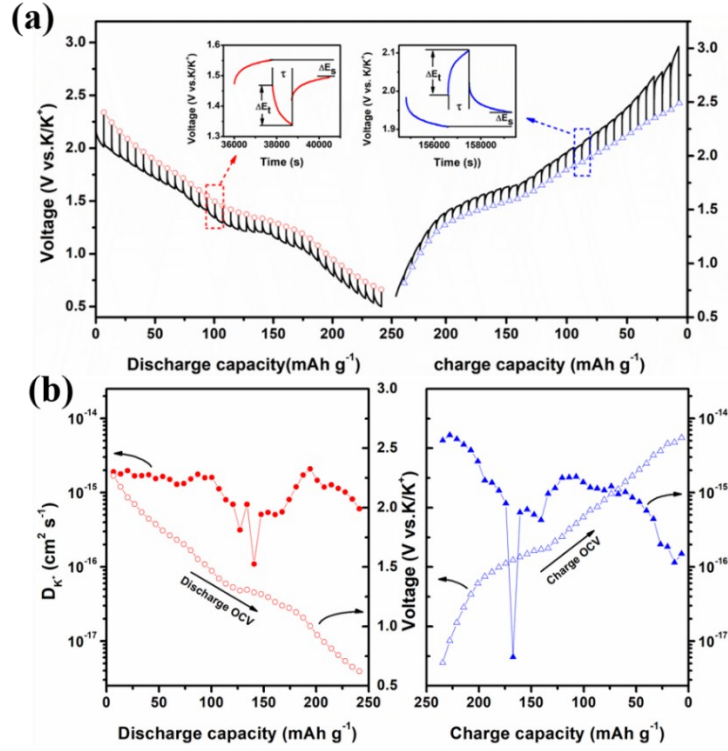


Figure S10 (a) Voltage profile and (b) K-ion diffusion coefficients of SeS₂-CPAN obtained via the GITT technique during discharge/charge process.

A constant current of 33 mA g⁻¹ is applied for 0.25 h before cells rest at open circuit for 0.5 h for each step. Figure S10a shows the quasi-equilibrium open-circuit-voltage (OCV) and transient voltage responses during the potassiation and depotassiation processes measured by GITT. From the transient voltage reposed during GITT measurement, the chemical diffusion coefficient D_k of potassium in the active material can be estimated according to equation (S1)

$$D_k = \frac{4}{\pi\tau} \left(\frac{n_M V_M}{S} \right)^2 \left(\frac{\Delta E_s}{\Delta E_t} \right)^2 \quad (\text{S1})$$

where τ is the duration of the current pulse (1800 s), ΔE_s and ΔE_t are the change of the voltages during a current pulse and after a current pulse (figure S10a inset), respectively, where n_M and V_M are the molar mass (mol) and volume (cm³/mol) of the SeS₂-CPAN active material, respectively, S is the surface area of a single particle¹. For the SeS₂-CPAN cathode, we assume that the solid phase consists of spherical particles with radius R_s of ~1×10⁻⁵cm, so Equation S1 becomes

$$D_k = \frac{4}{\pi\tau} \left(\frac{R_s}{3} \right)^2 \left(\frac{\Delta E_s}{\Delta E_t} \right)^2 \quad (\text{S2})$$

The calculated chemical diffusion coefficient of K-ion during potassiation and depotassiation is plotted in

Figure S10b and listed in Tables S2 and S3.

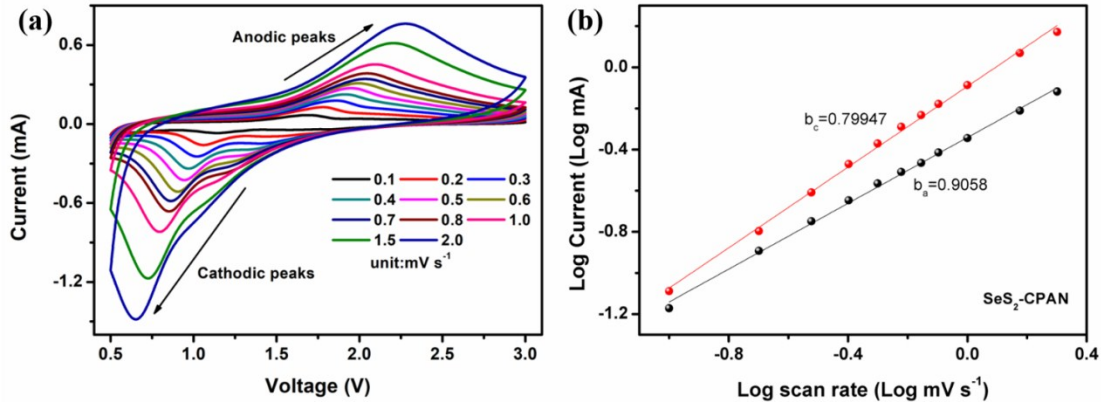


Figure S11. (a) CV curves of SeS₂-CPAN with scanning rates ranging from 0.1 to 2.0 mV s⁻¹. (b) Determination of the b-value using the relationship between peak current and scan rate.

Figure S11a show the CV curves at various scan rates from 0.1 to 2.0 mV s⁻¹, they display similar shapes with broad peaks during both cathodic and anodic processes. According to the relationship between the measured current (i) and the scan rate (ν):²⁻⁵

$$i = a\nu^b \quad (S3)$$

the b-value can be determined by the slope of the $\log(\nu)$ - $\log(i)$ plots. In particular, the b-value of 0.5 indicates a total diffusion-controlled behavior, whereas 1.0 represents a capacitive process. We analyze the redox peaks, and the plot of $\log(\nu) - \log(i)$ is presented in Figure S11b.

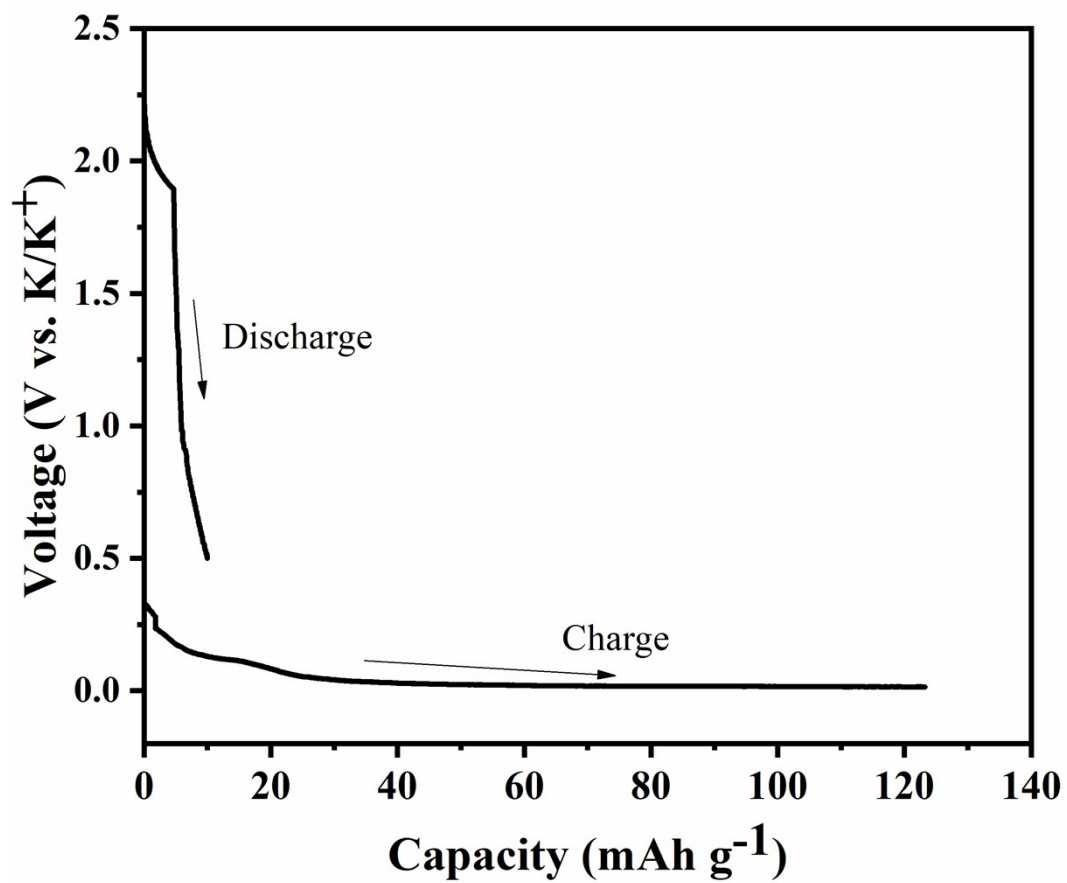


Figure S12. The initial charge/discharge curves of K-S battery with porous separator and liquid electrolyte at 50°C.

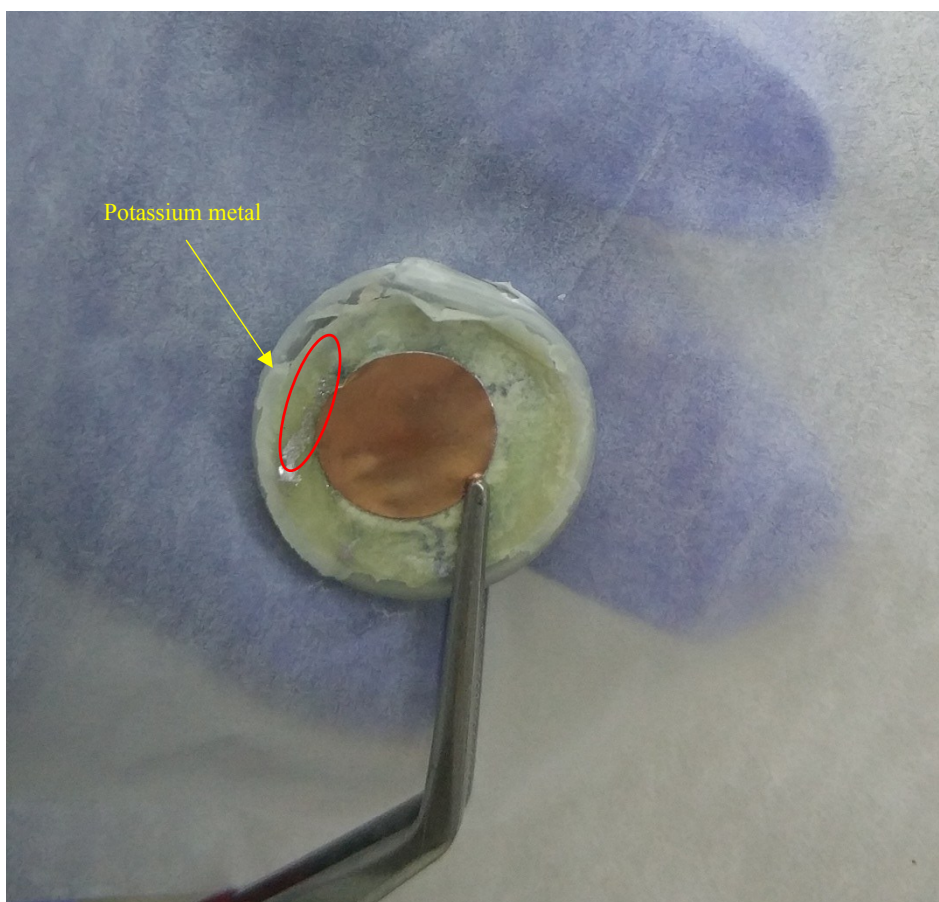


Figure S13. The optical images of K-S battery with glass fiber separator after cycled at 100 mA g^{-1} at 50°C .

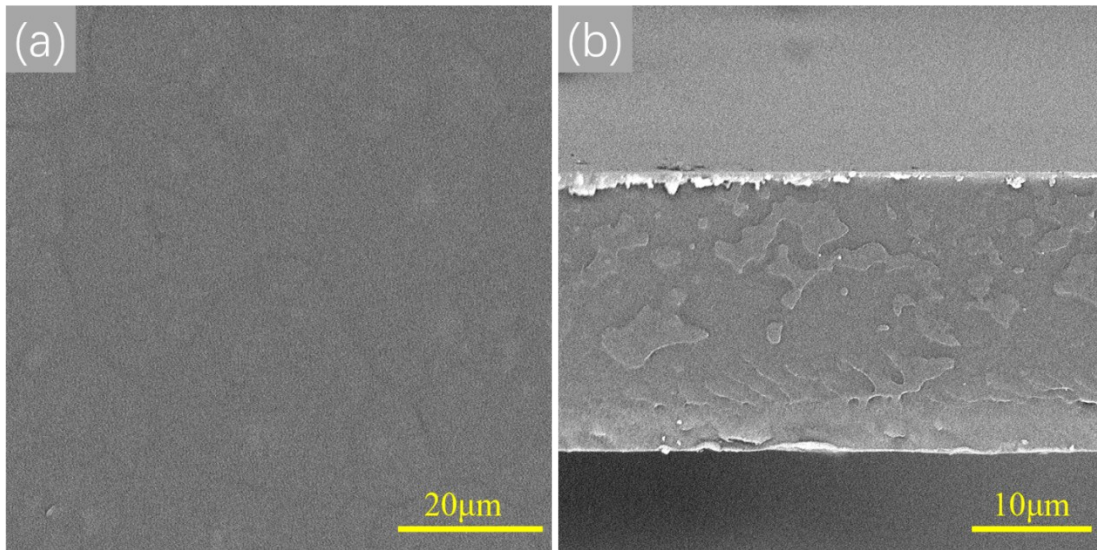


Figure S14. (a) Top view and (b) cross-section SEM images of the polymer membrane.

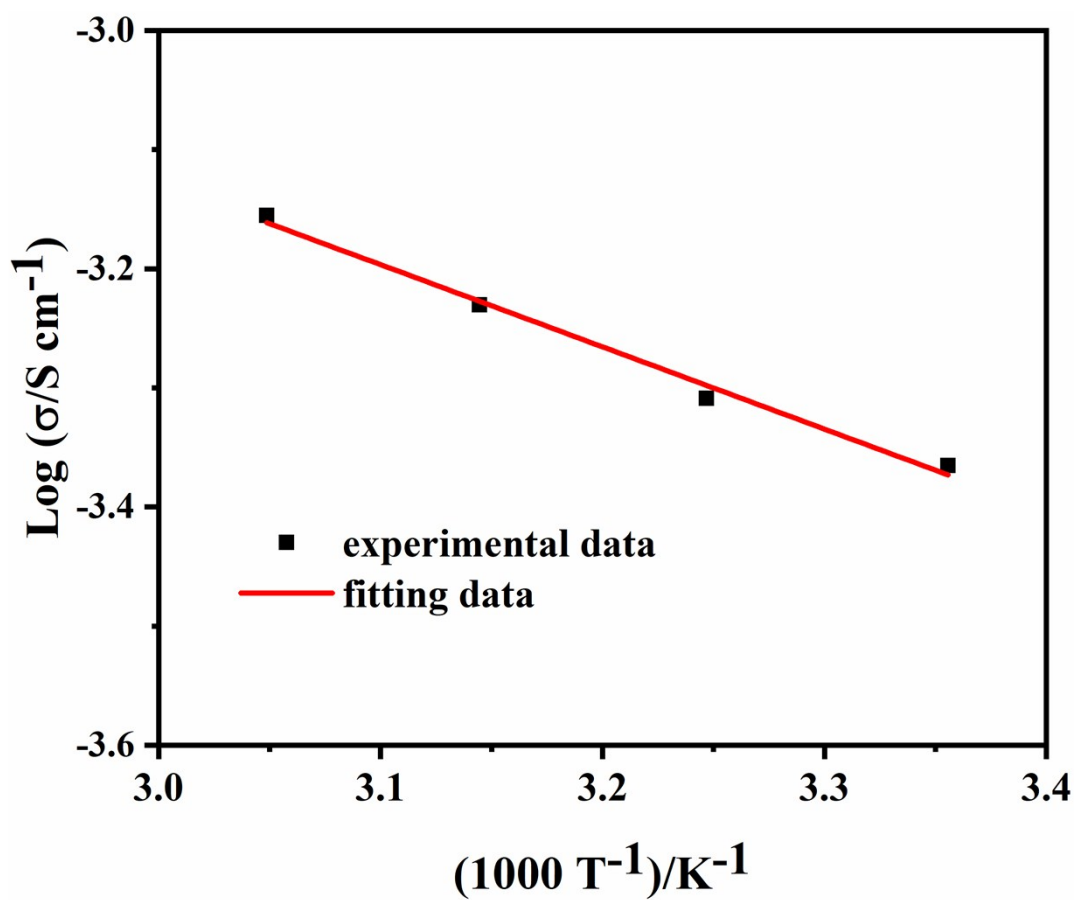


Figure S15. Ionic conductivity of the gel polymer electrolyte as a function of temperature.

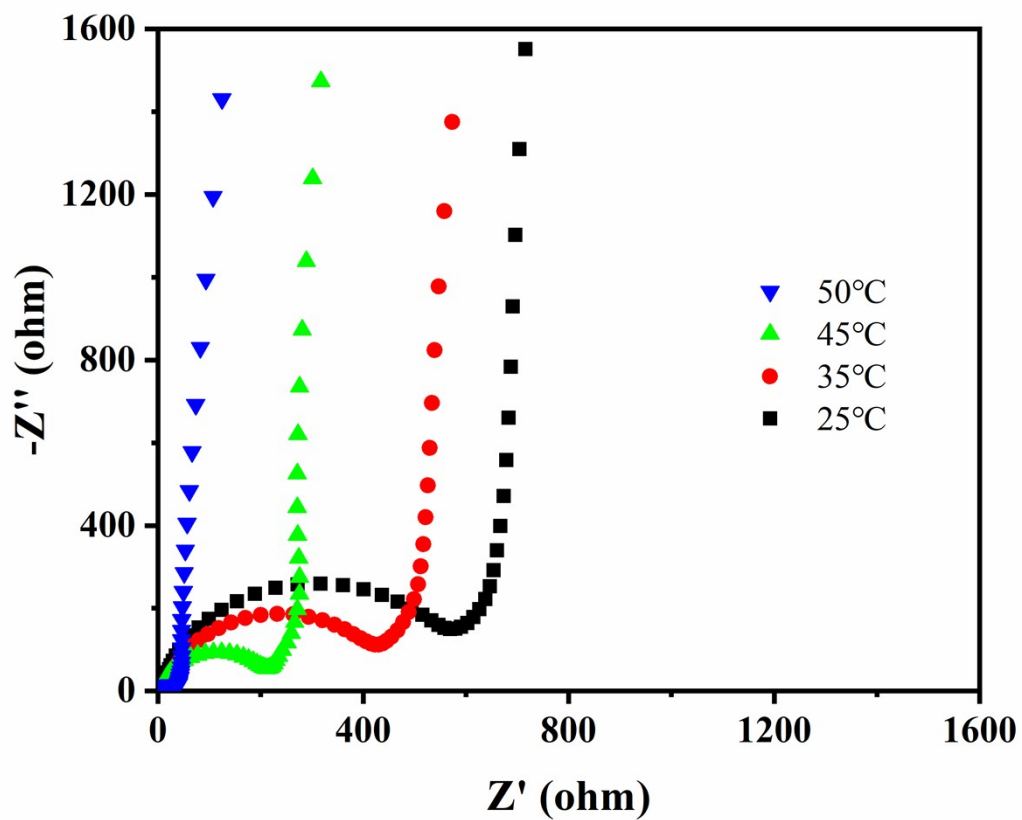


Figure S16. Nyquist plots of the potassium// SeS₂-CPAN cell with gel polymer electrolyte before cycling at different temperatures from 25 to 50°C.

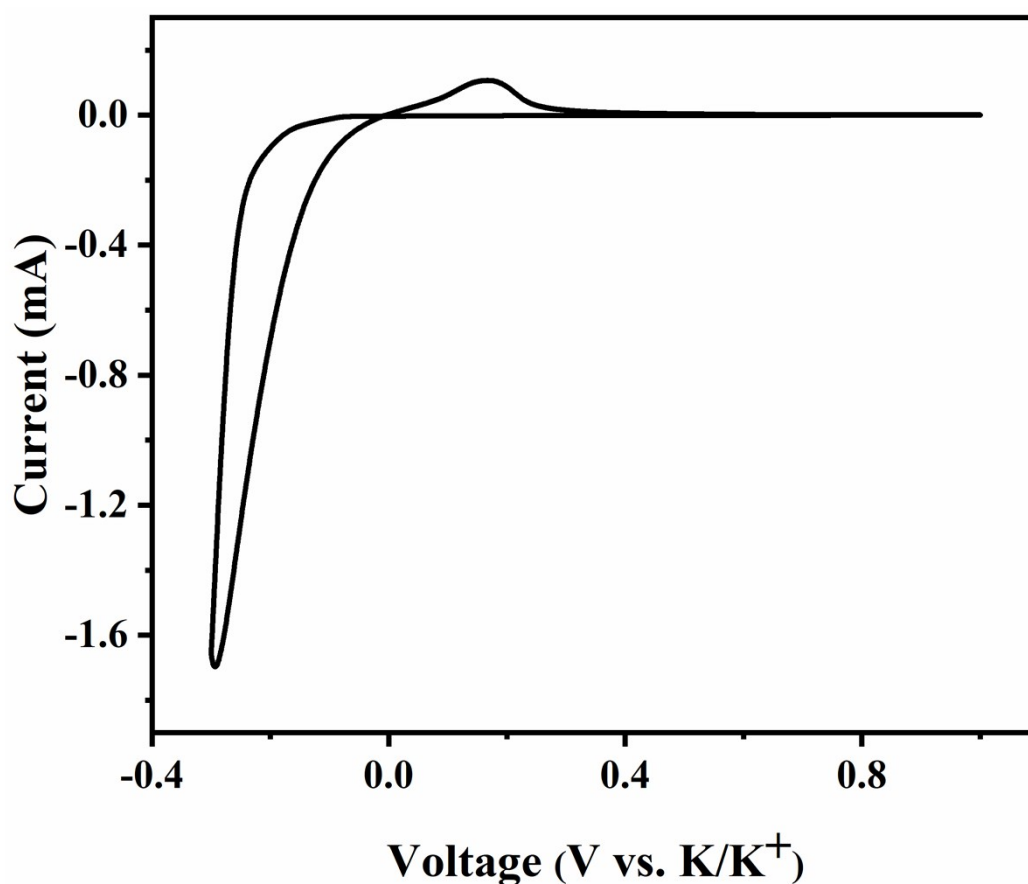


Figure S17. The plating/stripping behavior of potassium in a coin cell with the gel polymer electrolyte sandwiched between a potassium-metal and a stainless-steel electrode at a scan rate of 0.2 mV s^{-1} .

The behavior of potassium metal stripping/plating on stainless steel with the gel polymer electrolyte was tested via cyclic voltammetry with K metal as both the reference and counter electrodes and stainless steel as the working electrode.

The sharp cathodic peak at -0.3 V vs. K/K^+ corresponds to the plating of potassium on working electrode (stainless steel). The anodic peak at $0.21 \text{ V (vs. K/K}^+)$ represents the stripping of potassium from stainless steel.

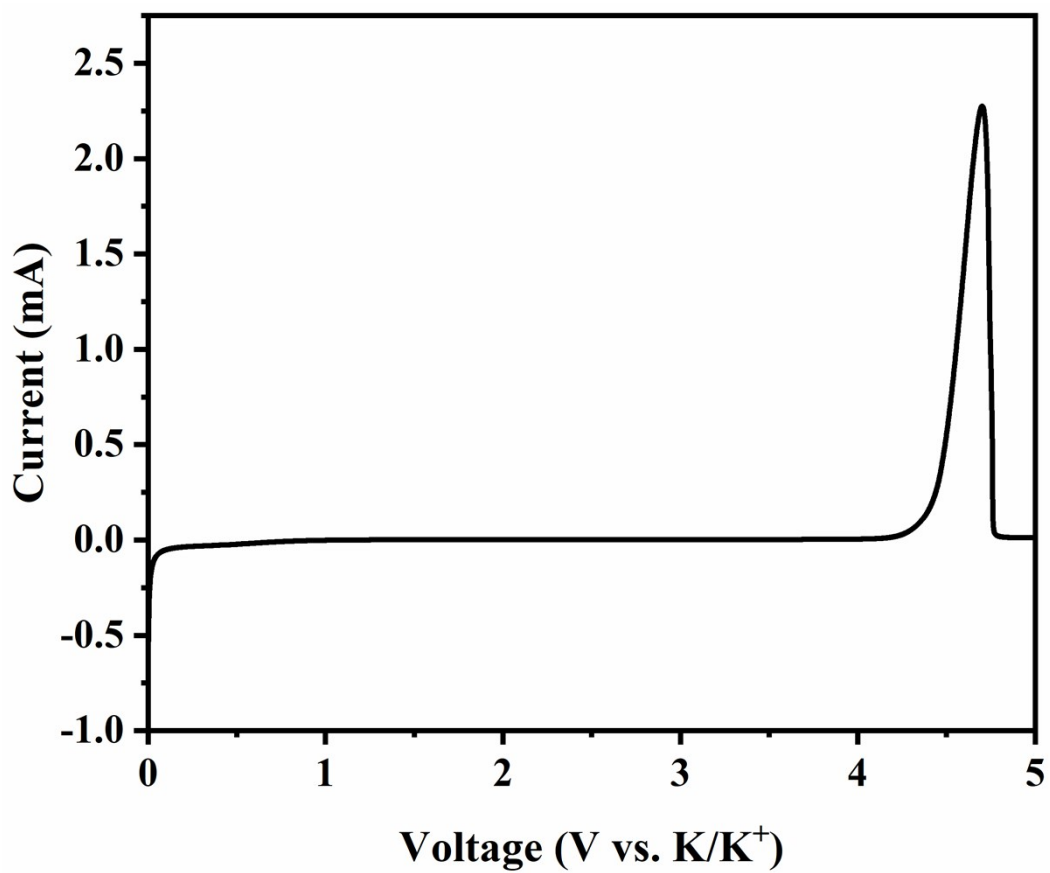


Figure S18. LSV plot of the gel polymer electrolyte sandwiched between a potassium-metal and a stainless-steel electrode at a scan rate of 1.0 mV s^{-1} .

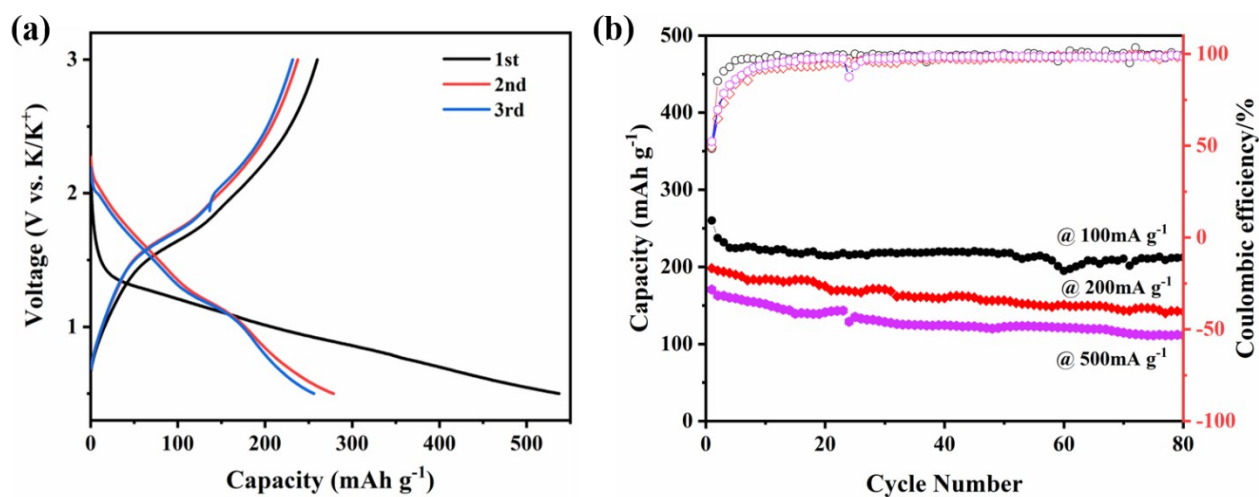


Figure S19. Electrochemical performance of SeS₂-CPAN toward potassium with gel polymer electrolyte at room temperature. (a) Galvanostatic charge and discharge curves at 100 mA g⁻¹ for the first three cycles, (b) cycling stability and coulombic efficiency of SeS₂-CPAN at 100, 200 and 500 mA g⁻¹.

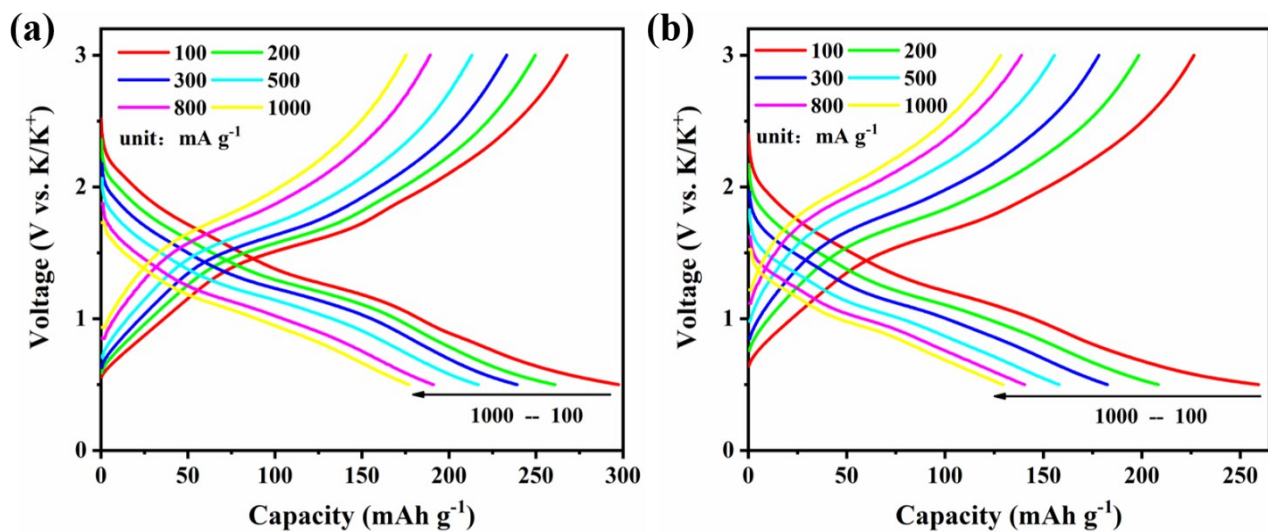


Figure S20. Electrochemical performance of SeS₂-CPAN toward potassium with gel polymer electrolyte. charge-discharge curves at various current rate under (a) 50 °C and (b) room temperature.

Table S1. Electrochemical performance comparison of the recent reported positive electrode materials for K-based batteries.

Materials	Voltage range(V)	Capacity/cycles/rate/retention (mAh g ⁻¹ /-/mA g ⁻¹ /%)	Capacity/rate (mAh g ⁻¹ /mA g ⁻¹)	References
SeS₂-CPAN	0.5-3.0	211.9/ 200/100/80.6 246.5/100/100/93.7	259.5, 100 210.3, 500 152.7, 2000	This paper
K _{0.5} V ₂ O ₅	1.5-3.8	72.2/80/20/90.3	89.9, 10 79.2, 50 45, 200 124, 50	6
K _{0.65} Fe _{0.5} Mn _{0.5} O ₂	1.5-4.2	~78/350/100/78	103, 100 34, 800	7
K ₃ V ₂ (PO ₄) ₃	2.5-4.3	52/100/20/-	54, 20 25, 200	8
KPBNPs	2.0-4.0	73.2/100/50/-	76, 50 46, 300 117, 50	9
PTCDA	1.5-3.5	90/200/50/-	92, 100 73, 500	10
PAQS	1.5-3.4	90/200/50/-	198,20	11
PANI@CMK-3/S	1.2-2.4	329.3 mAh g _s ⁻¹ /50/50/-	500, 50	12
Sulfur (150°C)	1.2-3.0	~300/100/2.31mA cm ⁻² /-	~400, 0.33mA cm ⁻² ~285, 3.3 mA cm ⁻²	13
PTCDA@450°C	1.5-3.5	98/1000/1000/86.7	~125, 100	14
Polysulfide catholyte	1.2-2.4	~320 mAh/g _s /20 /55.8/94	~300mAh/g _s , 111.6 ~100, 1116	15
KCrS ₂	1.8-3.0	43/1000/173/90	63,8.65 42,865	16
SPAN	0.8-2.9	147/100/125/53	162, 250 83, 750	17

Table S2. The calculated chemical diffusion coefficient for K (D_K) during potassiation (The data are also shown in Figure S10).

Discharge capacity (mAh g⁻¹)	D_k (cm² s⁻¹)	Discharge capacity (mAh g⁻¹)	D_k (cm² s⁻¹)	Discharge capacity (mAh g⁻¹)	D_k (cm² s⁻¹)
6.7	1.90359E-15	87.1	1.76284E-15	167.5	5.49666E-16
13.4	1.78717E-15	93.8	1.5837E-15	174.2	8.08697E-16
20.1	1.97899E-15	100.5	1.60135E-15	180.9	1.19705E-15
26.8	1.67816E-15	107.2	1.12841E-15	187.6	1.7253E-15
33.5	1.69152E-15	113.9	8.02842E-16	194.3	2.08676E-15
40.2	1.73775E-15	120.6	6.9441E-16	201	1.4652E-15
46.9	1.54444E-15	127.3	3.13659E-16	207.7	1.19011E-15
53.6	1.64574E-15	134	6.94668E-16	214.4	1.27123E-15
60.3	1.50436E-15	140.7	1.09187E-16	221.1	1.14146E-15
67	1.29128E-15	147.4	5.08647E-16	227.8	1.01546E-15
73.7	1.32548E-15	154.1	5.42282E-16	234.5	8.17846E-16
80.4	1.52414E-15	160.8	5.04507E-16	241.2	6.05249E-16

Table S3. The calculated chemical diffusion coefficient for K (D_K) during depotassiation (The data are also shown in Figure S10).

Discharge capacity (mAh g⁻¹)	D_k (cm² s⁻¹)	Discharge capacity (mAh g⁻¹)	D_k (cm² s⁻¹)	Discharge capacity (mAh g⁻¹)	D_k (cm² s⁻¹)
234.5	5.04684E-15	154.1	5.91772E-16	73.7	1.21461E-15
227.8	5.93395E-15	147.4	5.07253E-16	67	9.50866E-16
221.1	5.26353E-15	140.7	4.27157E-16	60.3	1.01749E-15
214.4	4.43301E-15	134	9.68329E-16	53.6	8.62046E-16
207.7	3.72482E-15	127.3	1.14784E-15	46.9	7.50131E-16
201	2.6222E-15	120.6	1.58546E-15	40.2	5.71886E-16
194.3	1.46035E-15	113.9	1.60812E-15	33.5	4.41112E-16
187.6	1.36886E-15	107.2	1.63363E-15	26.8	2.01585E-16
180.9	1.0668E-15	100.5	1.38236E-15	20.1	1.861E-16
174.2	7.17035E-16	93.8	1.17061E-15	13.4	1.14326E-16
167.5	6.09841E-18	87.1	1.13976E-15	6.7	1.50016E-16
160.8	5.42987E-16	80.4	1.0747E-15		

References

- 1 L. C. Zheng Shen, Christopher D. Rahn, and Chao-Yang Wang, *J. Electrochem. Soc.*, 2013, **160**, A1482.
- 2 V. Augustyn, J. Come, M. A. Lowe, J. W. Kim, P. L. Taberna, S. H. Tolbert, H. D. Abruna, P. Simon and B. Dunn, *Nat. Mater.*, 2013, **12**, 518-522.
- 3 J. Ding, H. Zhou, H. L. Zhang, L. Y. Tong and D. Mitlin, *Adv. Energy Mater.*, 2018, **8**.
- 4 Z. Li, J. Zhang, Y. Lu and X. W. D. Lou, *Sci. Adv.*, 2018, **4**, eaat1687.
- 5 H. W. Xuming Yang, Denis Y. W. Yu, and Andrey L. Rogach, *Adv. Funct. Mater.*, 2018, **28**, 1706609.
- 6 L. Deng, X. Niu, G. Ma, Z. Yang, L. Zeng, Y. Zhu and L. Guo, *Adv. Funct. Mater.*, 2018, **28**, 1800670.
- 7 T. Deng, X. Fan, J. Chen, L. Chen, C. Luo, X. Zhou, J. Yang, S. Zheng and C. Wang, *Adv. Funct. Mater.*, 2018, **28**, 1800219.
- 8 J. Han, G. N. Li, F. Liu, M. Wang, Y. Zhang, L. Hu, C. Dai and M. Xu, *Chem. Commun.*, 2017, **53**, 1805-1808.
- 9 C. Zhang, Y. Xu, M. Zhou, L. Liang, H. Dong, M. Wu, Y. Yang and Y. Lei, *Adv. Funct. Mater.*, 2017, **27**, 1604307.
- 10 Y. Chen, W. Luo, M. Carter, L. Zhou, J. Dai, K. Fu, S. Lacey, T. Li, J. Wan, X. Han, Y. Bao and L. Hu, *Nano Energy*, 2015, **18**, 205-211.
- 11 Z. Jian, Y. Liang, I. A. Rodríguez-Pérez, Y. Yao and X. Ji, *Electrochem. Commun.*, 2016, **71**, 5-8.
- 12 Q. Zhao, Y. X. Hu, K. Zhang and J. Chen, *Inorg. Chem.*, 2014, **53**, 9000-9005.
- 13 X. Lu, M. E. Bowden, V. L. Sprenkle and J. Liu, *Adv. Mater.*, 2015, **27**, 5915-5922.
- 14 L. Fan, R. Ma, J. Wang, H. Yang and B. Lu, *Adv. Mater.*, 2018, **30**, e1805486.
- 15 J.-Y. Hwang, H. M. Kim, C. S. Yoon and Y.-K. Sun, *ACS Energy Lett.*, 2018, **3**, 540-541.
- 16 N. Naveen, W. B. Park, S. P. Singh, S. C. Han, D. Ahn, K. S. Sohn and M. Pyo, *Small*, 2018, DOI: 10.1002/sml.201803495, e1803495.

17 Y. Liu, W. Wang, J. Wang, Y. Zhang, Y. Zhu, Y. Chen, L. Fu and Y. Wu, *Chem. Commun.*, 2018, **54**, 2288-2291.